Identification of a new subset of lymph node stromal cells involved in regulating plasma cell homeostasis

Hsin-Ying Huang[a], Ana Rivas-Caicedo[b,c,d], François Renevey[a], Hélène Cannelle[a], Elisa Peranzoni[b,c,d], Leonardo Scarpellino[a], Debbie L. Hardie[e], Arnaud Pommier[b,c,d], Karin Schaeuble[a], Stéphanie Favre[a], Tobias K. Vogt[a], Fernando Arenzana-Seisdedos[f], Pascal Schneider[a], Christopher D. Buckley[e,g], Emmanuel Donnadieu[b,c,d,1], and Sanjiv A. Luther[a,1,2]

[a]Department of Biochemistry, Center for Immunity and Infection, University of Lausanne, 1066 Epalinges, Switzerland; [b]INSERM, U1016, Institut Cochin, 75014 Paris, France; [c]CNRS, UMR8104, Institut Cochin, 75014 Paris, France; [d]Université Paris Descartes, Sorbonne Paris Cité, Institut Cochin, 75014 Paris, France; [e]Centre for Translational Inflammation Research, School of Immunity and Infection, University of Birmingham, Queen Elizabeth Hospital, Birmingham B15 2WD, United Kingdom; [f]Unité de Pathogénie Virale, Département de Virologie, INSERM U819, Institut Pasteur, 75015 Paris, France; and [g]Kennedy Institute of Rheumatology, University of Oxford, Oxford OX3 7FY, United Kingdom

Edited by Rafi Ahmed, Emory University, Atlanta, GA, and approved June 6, 2018 (received for review July 14, 2017)

Antibody-secreting plasma cells (PCs) arise rapidly during adaptive immunity to control infections. The early PCs are retained within the reactive lymphoid organ where their localization and homeostasis rely on extrinsic factors, presumably produced by local niche cells. While myeloid cells have been proposed to form those niches, the contribution by colocalizing stromal cells has remained unclear. Here, we characterized a subset of fibroblastic reticular cells (FRCs) that forms a dense meshwork throughout medullary cords of lymph nodes (LNs) where PCs reside. This medullary FRC type is shown to be anatomically, phenotypically, and functionally distinct from T zone FRCs, both in mice and humans. By using static and dynamic imaging approaches, we provide evidence that medullary FRCs are the main cell type in contact with PCs guiding them in their migration. Medullary FRCs also represent a major local source of the PC survival factors IL-6, BAFF, and CXCL12, besides also producing APRIL. In vitro, medullary FRCs alone or in combination with macrophages promote PC survival while other LN cell types do not have this property. Thus, we propose that this FRC subset, together with medullary macrophages, forms PC survival niches within the LN medulla, and thereby helps in promoting the rapid development of humoral immunity, which is critical in limiting early pathogen spread.

FRC subsets | lymph node medulla | extrafollicular B cell differentiation | plasma cell survival | humoral response

Lymph nodes (LNs) are specialized organs filtering lymph fluid and inducing adaptive immunity to antigens derived from pathogens, tumors, or vaccines. They are composed of different regions, each populated by distinct resident stromal cells, including follicular dendritic cells (FDCs), that attract recirculating B cells into follicles, and fibroblastic reticular cells (FRCs), that attract recirculating T cells and mature dendritic cells (DCs) into the paracortex (1, 2). The third compartment—the medulla—is a site of plasma cell (PC) residence and antibody secretion. So far, the stromal organizer cell of that zone has been poorly characterized.

PC responses are crucial for systemic antibody-mediated protection upon infection and are the main success reason of current vaccines. Upon B cell activation within LNs, two anatomical niches critical for an efficient humoral response develop: PC foci within medullary cords (MCs) and germinal centers (GCs) within follicles (3, 4). The extrafollicular B cell differentiation within MCs allows rapid antibody responses to limit systemic spread of replicating pathogens. Typically, within 2–4 d after infection, proliferating plasmablasts (PBs) are observed in outer T zones, which differentiate into PCs that take residence within MCs and secrete large quantities of antibodies. This early humoral response of lower affinity usually lasts a few days with only a small fraction of PCs surviving several weeks (3, 4). In contrast, the follicular B cell differentiation within GCs allows the generation of memory B cells and PCs of high affinity, with PCs exiting the LNs and homing to sites like the bone marrow (BM), where they can survive over months and provide long-term humoral protection starting around days 10 (d10) to d14 after immunization (4, 5).

PCs isolated from BMs, LNs, and spleen are mostly short lived when placed in vitro (6, 7), raising the question about the critical support cells providing extrinsic survival signals in vivo. The prevailing view is that myeloid cells, including macrophages, DCs, and granulocytes, mediate PC survival within activated LNs and spleen (4, 8). This is based both on evidence of colocalization in PC-rich areas and expression of factors which can increase PC survival in vitro, including BAFF, APRIL, IL-6, and CXCL12 (4, 6, 8). However, myeloid cells were found to be a minor source of BAFF and CXCL12 in vivo (8), consistent with an important role for nonhematopoietic cells as BAFF source in the extrafollicular PC response (9). In addition, in vivo cell-depletion experiments showed that myeloid cells have either a positive role (10), no role (11), or even a negative role in extrafollicular PC development (12).

In the BM, fibroblasts form part of the survival niche for long-lived PCs by producing IL-6 and CXCL12, along with hematopoietic cell types contributing BAFF and APRIL (4). Poorly characterized fibroblasts from LNs and spleen in mice and men were also shown to promote PC survival in vitro (7, 13–15),

Significance

Lymph nodes (LNs) are sites where adaptive immunity is initiated, leading to the generation of plasma cells (PCs) secreting large amounts of antibodies that typically interfere with pathogen spread. PCs are known to depend on extrinsic factors provided by niche cells to stay alive; however, the critical niche cells are still poorly understood. Here we present evidence for a fibroblast subset within murine and human LNs that is unique to the medulla where PCs reside. These fibroblasts produce factors that positively regulate PC homeostasis, similar to macrophages. Knowing the critical niche cells may help to design intervention strategies to target this niche in the setting of autoimmune disease caused by PCs secreting autoreactive antibodies.

Author contributions: H.-Y.H., F.R., H.C., T.K.V., C.D.B., E.D., and S.A.L. designed research; H.-Y.H., A.R.-C., F.R., H.C., E.P., L.S., D.L.H., A.P., K.S., S.F., T.K.V., E.D., and S.A.L. performed research; F.A.-S. and P.S. contributed new reagents/analytic tools; H.-Y.H., A.R.-C., F.R., H.C., E.P., L.S., D.L.H., A.P., S.F., T.K.V., E.D., and S.A.L. analyzed data; and H.-Y.H., E.D., and S.A.L. wrote the paper with contributions from all authors.

The authors declare no conflict of interest.

This article is a PNAS Direct Submission.

[1]E.D. and S.A.L. contributed equally to this work.

[2]To whom correspondence should be addressed. Email: Sanjiv.Luther@unil.ch.

This article contains supporting information online at www.pnas.org/lookup/suppl/doi:10.1073/pnas.1712628115/-/DCSupplemental.

Published online July 2, 2018.

raising the possibility that FRC-like cells within MCs may contribute to PC homeostasis.

FRCs expressing podoplanin (pdpn, also known as gp38) are found in all three peripheral LN (pLN) compartments, produce extracellular matrix (ECM) proteins, and are heterogeneous in their localization, morphology, and function (1, 16). T zone FRCs (TRCs) are the largest and best studied subset, forming a 3D cell network which physically guides lymphocyte migration (17). They support T cell function through the secretion of the survival factor IL-7 and the chemokines CCL19 and CCL21, responsible for T cell and DC attraction, motility, and retention within T zones (2, 16). TRCs wrap around a matrix-based tube system, called conduits, used for intranodal transport of lymph fluid and small molecules (18). Within follicles, two additional FRC subsets were described that express the naive B cell survival factor BAFF and the B cell attractant CXCL13: MAdCAM$^+$ marginal reticular cells (MRCs) localizing in the subcapsular region (19), and MAdCAM$^-$ FRCs in the outer follicle (20, 21). FRC depletion experiments have shown that lymphocyte responses cannot be induced efficiently in the absence of FRCs (22). Together, these data demonstrate that distinct FRC types act as organizer cells of microenvironments found within the B and T zones, and thereby play a critical role in adaptive immunity.

Given that matrix fibers and pdpn$^+$ FRC-like cells have been observed by histology within MCs by us and others (10, 18, 23–25), we hypothesized that a specialized FRC subset may serve as the missing positive regulator of local PC niches. Here, we have performed a detailed histological and functional analysis of FRC subsets within activated LNs. We report the identification of medullary FRCs (MedRCs) along with the characterization of their unique morphological, molecular, and functional properties. Importantly, using histological and functional assays, we demonstrate that MedRCs are a major structural component of the PC niche in the medulla guiding PC migration and residence, but also a potent source of PC attraction and survival factors.

Results

Histological Identification of Medullary FRCs in Murine and Human LNs. To generate a strong PC accumulation within LNs, mice were immunized s.c. with ovalbumin (OVA) protein in Montanide (Mont) adjuvant. After 5 to 8 d, strongly enlarged medullary areas were observed, composed of LYVE1$^+$ medullary sinuses (MSs) and MCs enriched in CD138$^+$ PCs, but only a few scattered B and T cells (Fig. 1 *A* and *B*). Networks of pdpn$^+$ desmin$^+$ FRCs and laminin$^+$ matrix structures were not only observed throughout T zones but also within MCs, often organizing around CD31$^+$ high endothelial venules (Fig. 1 *B* and *C* and *SI Appendix*, Fig. S1*A*). Similar to TRCs, reticular cells of the MCs express desmin, αSMA, and LTβ-receptor (*SI Appendix*, Fig. S1*B*). CD11b$^+$ or CD169$^+$ macrophages were predominantly seen within MSs, with some being inside MCs (Fig. 1*C*). When screening various stromal cell antibodies, we noted that BP3 (CD157) labels both MRCs and TRCs, but not MedRCs (Fig. 1*D* and *SI Appendix*, Fig. S1*C*), while MAdCAM-1 marks only MRCs in naive and activated lymph nodes. Thus, the combination of MAdCAM-1 and BP3 allows the distinction of MedRCs from TRCs and MRCs in murine LNs. CD34, however, marks only a subset of MedRCs found close to medullary blood vessels (*SI Appendix*, Fig. S1*D*).

Next, we assessed whether in human reactive LN sections these stromal cell markers would identify a similar MedRC subset colocalizing with PCs. Medullary regions were readily observed, displaying MCs densely populated by nucleated cells and centered around CD31$^+$ blood vessels while being surrounded by LYVE1$^+$ MSs harboring a few cells in the lumen (Fig. 1*E*). CD138$^+$ PCs localize preferentially to the MC, clearly separated from most T and B cells. As expected (26), pdpn shows the strongest expression on TRCs, which were CD21$^-$, while FDCs coexpress pdpn and CD21 (Fig. 1*F*). Within MCs, pdpn labels reticular cells, as well as vascular cells expressing CD31 and/or LYVE1 (Fig. 1*E*). In contrast to the mouse, BP3 expression is highest in the medulla, intermediate on TRCs, and low on FDCs (Fig. 1*F* and *SI Appendix*, Fig. S1*E*). Within MCs, BP3 expression was observed on a dense reticular cell network that partially colocalizes with pdpn$^+$ cells. Consistent with them being fibroblastic cells, MC regions display collagen I and laminin-expressing reticular fibers. They are part of the PC niche (Fig. 1*G*), as are CD11c$^+$ DCs and lysozyme$^+$ macrophages/granulocytes (*SI Appendix*, Fig. S1*F*). Thus, the PC niche composition in human LN medulla closely resembles the one observed in mice.

Identification of Medullary FRCs by Flow Cytometry. Next, the surface markers MAdCAM-1 and BP3 were tested by flow cytometry on CD45$^-$35$^-$31$^-$pdpn$^+$ FRCs isolated from murine LNs. Three FRC subsets were observed in both naive and activated LNs, with MAdCAM$^+$BP3$^+$ MRCs representing 5–10%, MAdCAM$^-$BP3$^+$ TRCs representing 50–65%, and MAdCAM$^-$BP3$^-$ MedRCs 20–35% of isolated FRCs (Fig. 2*A*). During immune response only MRCs slightly increased in proportion, with all subsets increasing fourfold in number and 40–80% of cells having incorporated BrdU (Fig. 2 *B* and *C* and *SI Appendix*, Fig. S2 *A* and *B*).

Given the distinct immune cell composition in MCs, we reasoned that MedRCs should be functionally different from CCL21$^+$ TRCs and CXCL13$^+$ MRCs. Indeed, MedRCs from both naive and activated LNs showed very little intracellular CCL21 protein, while many TRCs from wild type (WT), but not CCL19/21ser-deficient *plt/plt* mice, were CCL21$^+$ (Fig. 2*D* and *SI Appendix*, Fig. S2*C*). While some MRC-like cells express CCL21, other MRCs showed higher CXCL13 expression than TRCs, with MedRCs being CXCL13$^-$. This chemokine expression pattern was largely maintained during the immune response (*SI Appendix*, Fig. S2*D*). These findings were confirmed in sorted cells at the transcriptional level. *ccl21* and *cxcl13* mRNA were highest in TRCs and MRCs of naive and activated LNs, as were *ccl19* and *il7* (Fig. 2*E* and *SI Appendix*, Fig. S2*E*). Importantly, MedRCs had at least 10-fold lower levels of these four cytokine transcripts. In contrast, *cxcl12* was expressed mainly by MedRCs and TRCs. Sorted lymphatic and blood endothelial cells (LECs/BECs), however, did not show much expression for any of these cytokines. These qRT-PCR data corroborate with in situ hybridization (ISH) analysis, showing the very modest expression levels of *ccl21*, *cxcl13*, and *ccl19* transcripts within MCs, while *cxcl12* transcripts were found to be at levels comparable to the T zone (Fig. 2*F* and *SI Appendix*, Fig. S2*F*). Histological staining for chemokine proteins confirmed the lack of CCL21 and CXCL13 within MCs, while CXCL12 was readily detected, both in MCs and T zones, and frequently colocalizing with reticular pdpn$^+$ FRCs (Fig. 2*G*). Thus, our data demonstrate that MedRCs are anatomically, phenotypically, and functionally distinct from TRCs and MRCs. Multiparameter analysis by flow cytometry confirms this notion and indicates an even greater diversity of pdpn$^+$ fibroblastic LN cells than previously anticipated, with a continuum of seven phenotypically different FRC populations (Fig. 2*H* and *SI Appendix*, Fig. S2*G*), which do not include FDC and pdpn$^-$CD31$^-$ populations.

MedRCs and TRCs Generate Different ECM Structures. TRCs produce functional conduits that they enwrap but it is not known whether similar features apply to MedRCs. We observed a reticular staining for collagen I and IV as well as fibronectin, often in thinner structures than inside T zones but often colocalizing with pdpn$^+$ MedRCs (Fig. 3*A*). Consistent with these findings, all three FRC subsets express high levels of *collagen1α1* and *collagen1α2* transcripts, with a marked increase after immunization, especially in MedRCs (Fig. 3*B*). Given the high specificity of collagen I expression for fibroblasts, we used transgenic mice expressing GFP under control of the collagen 1α1 promoter (pCol-GFP) (27) to visualize FRCs in vivo. In activated LNs, a reticular GFP expression was clearly visible, being strongest in MCs, intermediate inside T zones, and absent in the center of follicles (Fig. 3*C*). By histology and flow cytometry GFP expression is largely restricted to the three FRC subsets (*SI Appendix*, Fig. S3 *A–D*). Similar to GFP expression, histological PDGFRα staining was stronger on

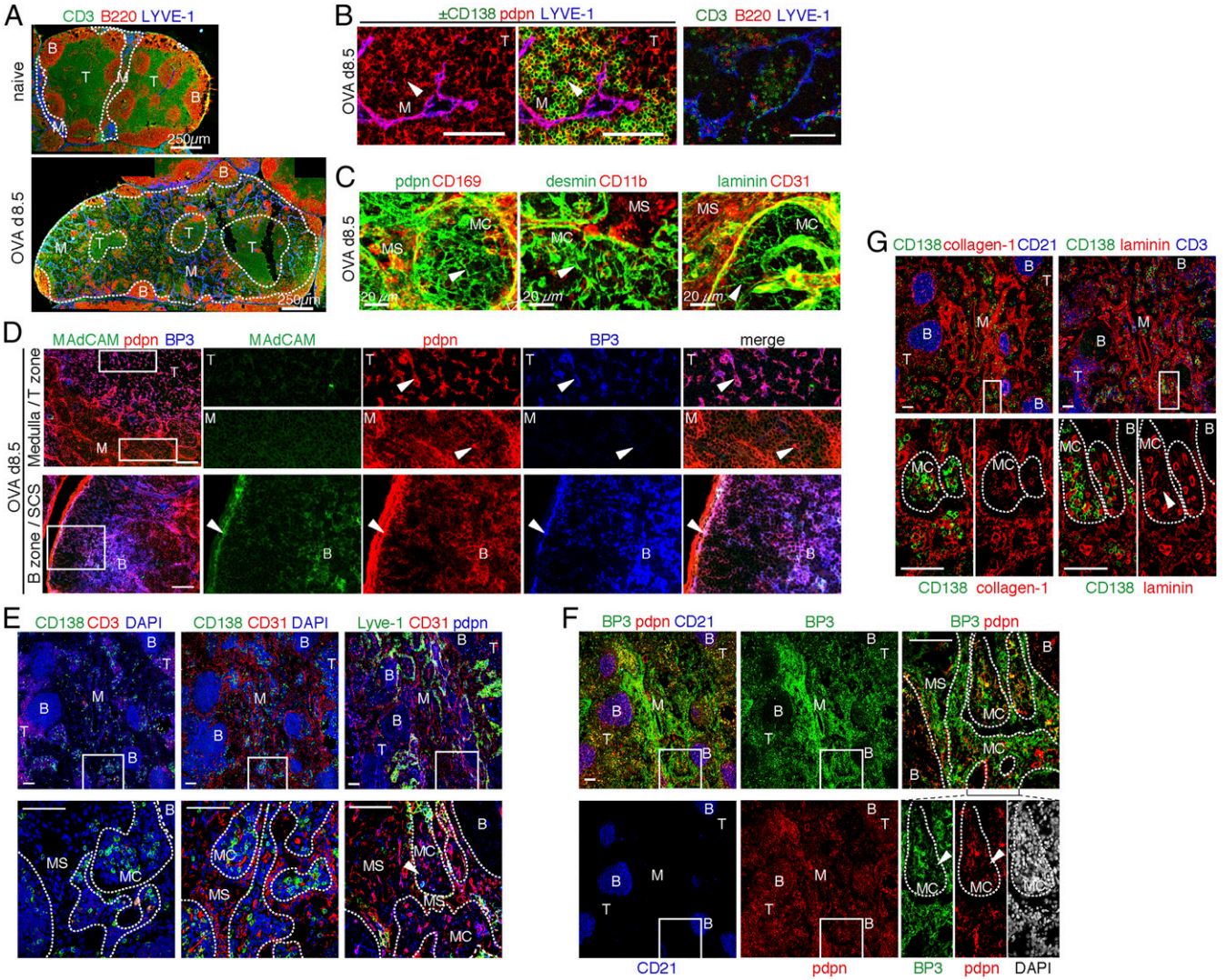

Fig. 1. Histological identification and characterization of a FRC subset colocalizing with plasma cells in medullary cords of activated lymph nodes. Immunofluorescence microscopy of sections from pLNs of naive or OVA/Mont-immunized mice (*A–D*), or on sections from human pLNs (*E–G*). (*A* and *B*) Cryostat sections stained for FRCs (pdpn$^+$LYVE1$^-$), lymphatic vessels (pdpn$^+$LYVE1$^+$), CD3$^+$ T cells, B220$^+$ B cells, and CD138$^+$ PCs. (*C* and *D*) Vibratome and cryostat sections of LNs stained with indicated antibodies. (*E–G*) Sections of human pLNs were stained for the indicated markers, with a focus on lymphoid compartments and vascular cells (*E*), fibroblastic cells (*F*), and extracellular matrix components (*G*). Boxed areas are shown at higher magnification at *Right* or the row *Below*. Dashed lines indicate examples of MCs where PCs reside. Arrows point to representative FRCs within a given zone. B, B cell zone (follicle); M, medulla; MC, medullary cord; MS, medullary sinus; SCS, subcapsular sinus; T, T cell zone. (Scale bar, 100 μm.) Results are representative of at least three independent mice or human samples.

MedRCs than TRCs, while BP3 and CCL21 showed the opposite pattern (Fig. 3*D* and *SI Appendix*, Fig. S3 *D–G*). This segregation was reflected in the lymphocyte distribution, with T cells colocalizing with CCL21$^+$ TRCs and scattered B cells found among MedRCs (*SI Appendix*, Fig. S3 *D* and *F*).

The increased GFP signal detected by fluorescence microscopy in MCs relative to T zones correlated with a twofold higher FRC density and therefore a reduced spacing between FRC processes (Fig. 3*E* and *SI Appendix*, Fig. S3*E*). In addition, MedRCs display less elongated cell bodies and thinner cell processes than TRCs (Fig. 3*E*). Similar to the collagen I staining, second harmonic generation (SHG) revealed differences in the fibrillar collagen organization. In the medulla, thick and wavy collagen bundles alternate with very thin fibers, while in T zones, collagen fibers display a more linear and regular organization (Fig. 3 *F* and *G* and Movie S1). Interestingly, MedRCs enwrapped less the matrix structures than did TRCs (Fig. 3*G*). To test conduit function, fluorescent dextran was injected s.c. While most tracer localized to LYVE1$^+$ MSs and to T zone conduits, a thin reticular pattern was apparent in MCs, overlapping with collagen IV staining (Fig. 3*H* and *SI Appendix*, Fig. S3*H*). In conclusion, MedRCs build a very dense cell network that is only partially associated with an equally dense but functional conduit network.

Medullary FRCs Show Extensive Contacts with PCs. Next, we compared the relative contribution of hematopoietic cells versus MedRCs to the PC niche. Numerous macrophages (F4/80$^+$, CD11b$^+$, or CD169$^+$), DCs (CD11c$^+$, MHCII$^+$), and B220$^+$ B cells are present in MCs and show direct PC contact, while the frequency of granulocytes (Gr1^{hi}) is much lower (Fig. 4*A* and *SI Appendix*, Fig. S4*A*). MedRCs were observed in MCs in a similar density as macrophages (*SI Appendix*, Fig. S4*B*). While 60–70% of PCs physically interacted with macrophages and B cells, almost 100% of PCs contacted GFP$^+$ MedRCs (Fig. 4*A*). The latter finding was confirmed and extended using 3D confocal image stacks, where on average 25% of the PC surface was found to physically touch MedRCs, often at multiple points (*SI Appendix*, Fig. S4*C* and Movie S2). Despite forming a dense network in

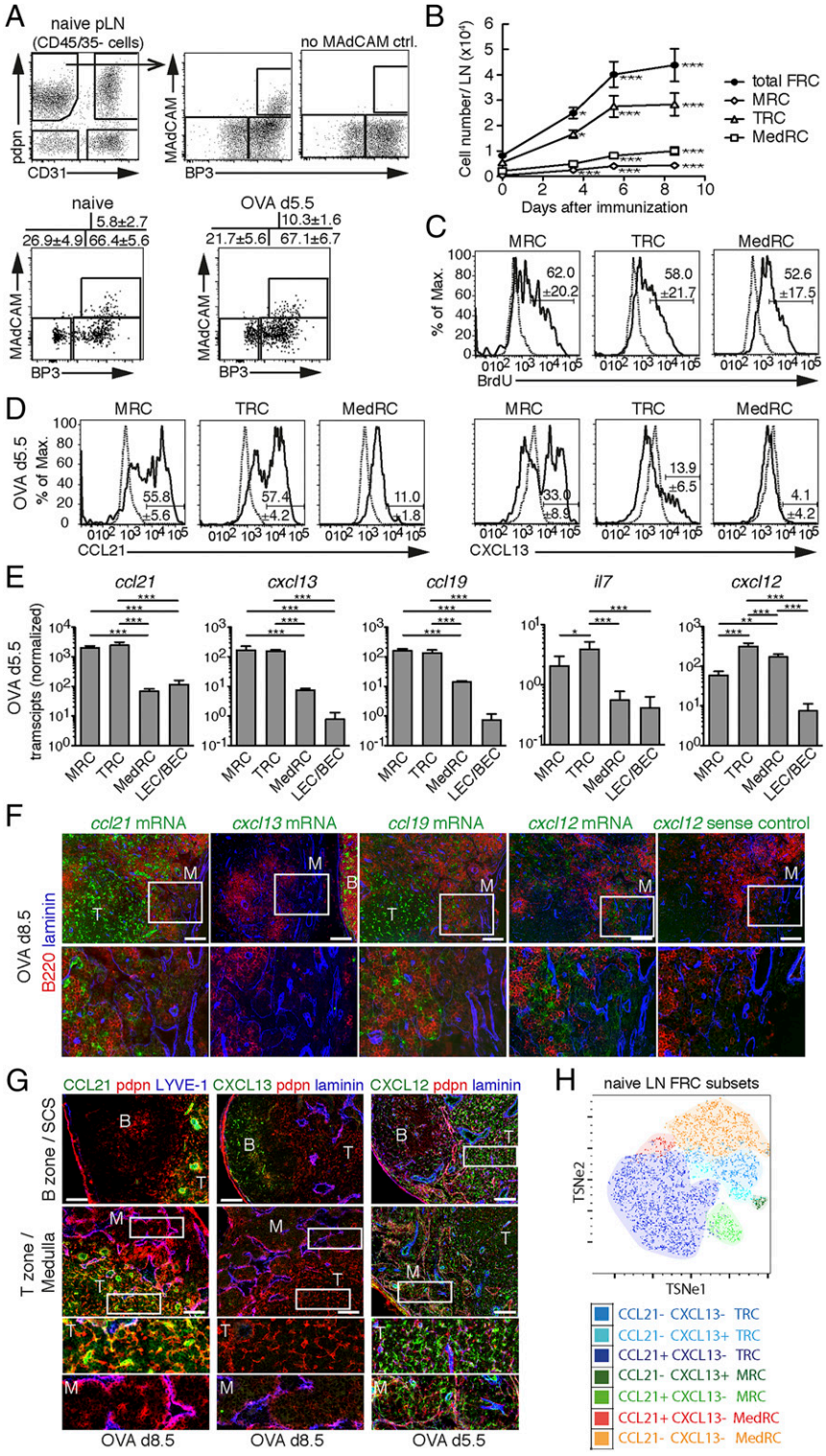

Fig. 2. Medullary FRCs have a unique phenotype and cytokine profile and expand in number during lymph node swelling. (*A–D*) FACS analysis of CD45$^-$CD35$^-$ cells from pLNs of naive or OVA/Mont-immunized mice at the indicated time points. (*A*) Dot plots in *Upper* row show the gating of FRCs (pdpn$^+$CD31$^-$) versus BECs (pdpn$^-$CD31$^+$) and LECs (pdpn$^+$CD31$^+$) from naive pLNs. The expression of MAdCAM and BP3 in FRCs distinguishes three FRC subpopulations: MRCs, TRCs, and MedRCs. Shown at *Right* is the control staining when anti-MAdCAM antibody was not added. Dot plots in *Lower* row show a representative staining of the three FRC subsets in naive versus activated LNs, with the percentages indicated for each population ($n \geq 3$). (*B*) Number of total FRCs and of each of the three FRC subsets per pLN upon immunization. (*C*) Representative histograms showing the level of BrdU incorporation in the three FRC subsets (OVA/Mont d5.5). Numbers indicate the percentage of BrdU$^+$ cells. Black line, anti-BrdU antibody; dashed line, isotype control antibody on total FRCs. (*D*) Representative histograms displaying the frequency of CCL21- and CXCL13-expressing cells among the three FRC subsets found in activated pLNs. Black line, specific antibody; dashed line, no primary antibody on total FRCs. (*E*) The three FRC subsets and CD31$^+$ cells (LECs/BECs) were sorted from activated pLNs and normalized transcript levels of indicated cytokine transcripts measured by qRT-PCR (means ± SD, $n = 4$). (*F*) ISH analysis for indicated cytokine transcripts (green) or the sense control (for CXCL12). (*G*) pLN sections stained with the indicated antibodies. The boxed areas are represented *Below* at higher magnification. (*H*) Multiparameter flow cytometry-based clustering of FRC (CD45$^-$31$^-$pdpn$^+$) subsets from naive pLNs using the TSNe algorithms (FlowJo) to display seven parameters (FCS, SSC, Pdpn, BP3, MAdCAM-1, CXCL13, and CCL21) in a 2D representation. Colored areas were added manually. (Scale bar, 100 μm.) Results in *A–D*, *F*, and *G* are representative of at least three independent mice. *$P < 0.05$, **$P < 0.01$, ***$P < 0.001$.

MCs, MedRCs do not contact all cells equally, as only 70% of B220$^+$ cells contact them, in contrast to 100% of PCs and F4/80$^+$ cells (*SI Appendix*, Fig. S4*D*).

To gain insight into the dynamics of PCs interactions with MedRCs, labeled PCs (CD138$^+$B220^{low}) or PBs (CD138$^+$B220^{int}) were added on top of viable tissue slices of activated LNs from pCol-GFP mice. Most PBs migrated preferentially into the MCs where endogenous CD138$^+$ PCs resided (*SI Appendix*, Fig. S4*E*). As previously reported (28), PBs showed higher motility than PCs, more prominently within the outer T zone than the MCs, and this migration was largely unaffected by pertussis toxin, which blocks most chemokine-based cell migration. Next, endogenous PCs/PBs within viable LN slices were antibody labeled to image their dynamic interaction with GFP$^+$ FRCs. In the outer T zone, PBs moved rapidly and often in long linear tracks, thereby following the TRC network, going from one TRC to the next, but with no directional bias toward MCs (Fig. 4 *B* and *C*, *SI Appendix*, Fig. S4*F*, and Movies S3 and S4). In contrast, PCs in

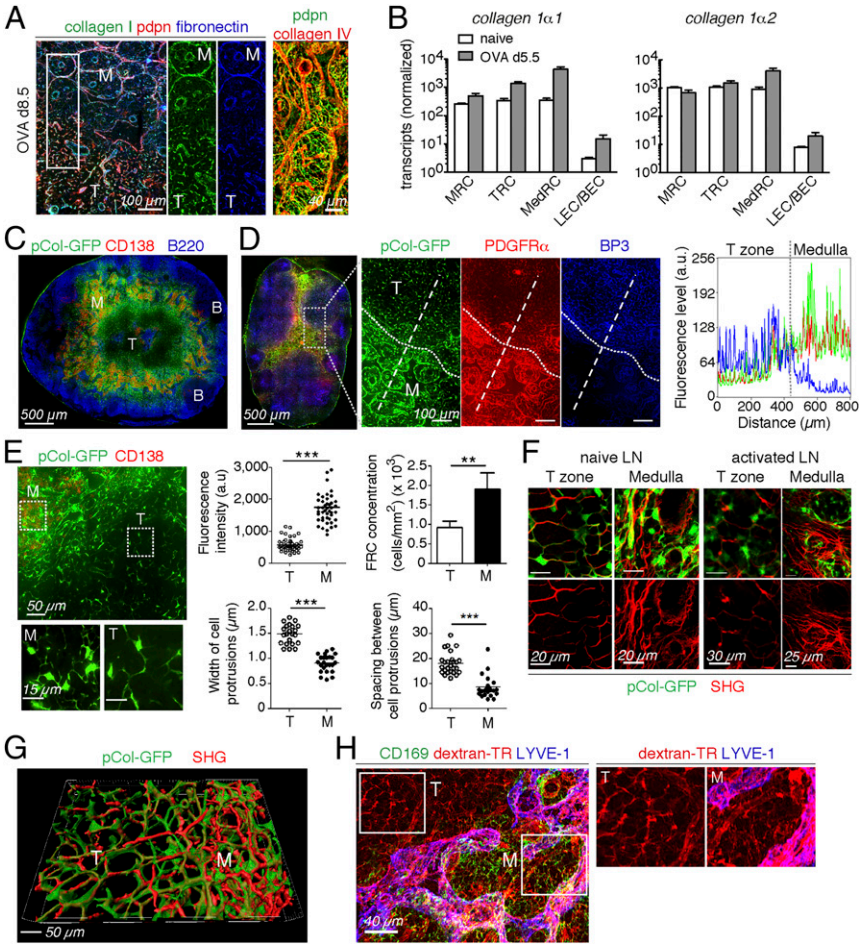

Fig. 3. Medullary FRCs produce a dense matrix network and only partially associate with it. (*A*) Immunofluorescence microscopy of activated pLNs (OVA/Mont d8.5) for the indicated antibodies. The boxed area is represented in the *Middle* at higher magnification and with single colors. Shown at *Right* is a vibratome section of the LN medulla. (*B*) The levels of collagen 1α1 and collagen 1α2 transcripts are shown for the indicated cell types isolated from either naive or activated (OVA/Mont d5.5) pLNs (means ± SD, $n = 4$). (*C–E*) Confocal images of vibratome sections of pLNs (SRBC d7) from pCol-GFP mice and stained with the indicated antibodies. (*D*) Histogram showing the fluorescence intensity of each marker along the dashed line (*Right*). (*E*) The boxed areas are represented *Below* at higher magnification and showing only the GFP$^+$ fibroblasts either in T zone or medulla. Graphs at *Right* show the GFP fluorescence intensity of FRCs found in these two zones, their concentration, as well as the width and spacing between fibroblast protrusions. $^{**}P < 0.01$, $^{***}P < 0.001$. (*F*) Two-photon microscopy images of naive and activated pLNs (SRBC d7) from pCol-GFP mice showing GFP expression and SHG highlighting collagen fibers. (*G*) Three-dimensional reconstruction of two-photon images displaying T zones and MCs of naive LNs. See also Movie S1. (*H*) Vibratome section of pLNs (OVA/Mont d5.5) 10 min after s.c. injection of Texas Red (TR)-dextran and stained with the antibodies indicated. The boxed areas are represented at *Right* at higher magnification.

MCs showed much slower and confined migration with limited displacement (Fig. 4 *B* and *C* and Movie S5). Consequently, PC interactions with each MedRC were considerably longer, changes from one MedRC to the other less frequent, and contact always continuous. MedRCs frequently showed pronounced morphological changes, in contrast to the more static TRCs (Movie S6), possibly due to the difference in matrix association. Collectively, these data show that MedRCs physically guide PC migration and residence, by providing both a cellular network and niche-like structures.

Medullary FRCs Are a Rich Source of Plasma Cell Survival Factors. To look for the potential expression of PC survival factors by MedRCs, they were sorted along with seven other cell types. Strikingly, on d5- and d8-activated LNs, *baff* transcripts were 40- to 100-fold more abundant in the three FRC subsets than in macrophages and DCs, with rare granulocytes showing intermediate levels (Fig. 5*A* and *SI Appendix*, Fig. S5 *A* and *B*). In contrast, *april* transcript levels were similar among FRC subsets, macrophages, and DCs. *Il6* transcripts were 10- to 20-fold higher in MedRCs than in other FRC subsets and myeloid cells. Finally, *Cxcl12* was highly enriched in the three FRC subsets. Surprisingly, expression of these four cytokines were similar in cells sorted from activated versus naive LNs (*SI Appendix*, Fig. S5*B*), pointing to an increase in the number of expressing cells rather than expression levels.

Given that we saw a preferential expression of BAFF and IL-6 transcripts in FRCs, especially MedRCs, we wished to localize them in sections of activated LNs, similar to our previous analysis for CXCL12 (Fig. 2 *F* and *G*). BAFF protein staining of activated WT LNs was strongest within MCs, with lower expression detectable within T and B zones. Part of the medullary BAFF colocalized with pdpn$^+$ FRCs. To identify the BAFF source more precisely, activated LNs of mice transgenic for a noncleavable BAFF were investigated. Strikingly, the BAFF staining was much stronger than in WT LNs, with highest levels on pdpn$^+$/desmin$^+$ MedRCs and TRCs (Fig. 5*B* and *SI Appendix*, Fig. S5 *C* and *D*). IL-6 transcripts were also abundantly present within MCs, besides their expression in B and T zones (Fig. 5*C*). To further define the cellular sources of IL-6 and BAFF at the protein level, various cell types were sorted, cultured, and assessed by ELISA. Ex vivo MedRCs proved to be the richest source of IL-6 protein compared with TRCs, macrophages, and DCs (Fig. 5*D*). In contrast, we failed to detect secreted or surface bound BAFF. Thus, our results suggest that within the PC niche, MedRCs are a major source of IL-6, BAFF, and CXCL12, with hematopoietic cells contributing only APRIL and possibly IL-6 at comparable levels.

IL-6 Is Important for Plasma Cell Differentiation or Survival in Peripheral LNs. Given the predominant IL-6 expression by MedRCs, we tested the in vivo role of IL-6 for the extrafollicular PC response. IL-6 competent splenocytes from OT-I and OT-II TCRs, transgenic (tg) mice were transferred into IL-6–deficient mice followed by OVA/Mont immunization, which allowed a normal T cell expansion (*SI Appendix*, Fig. S6*A*). On d5.5 and d8.5 after immunization, PB/PC numbers in the draining LNs were reduced by 60% in IL-6 KO mice relative to controls (Fig. 6*A* and *SI Appendix*, Fig. S6*A*). This result cannot be explained by altered B cell development in IL-6 KO mice, because transferred WT B cells showed a similar reduction in local PB/PC differentiation as IL6$^{-/-}$ B cells. We noted a marked reduction in various stromal

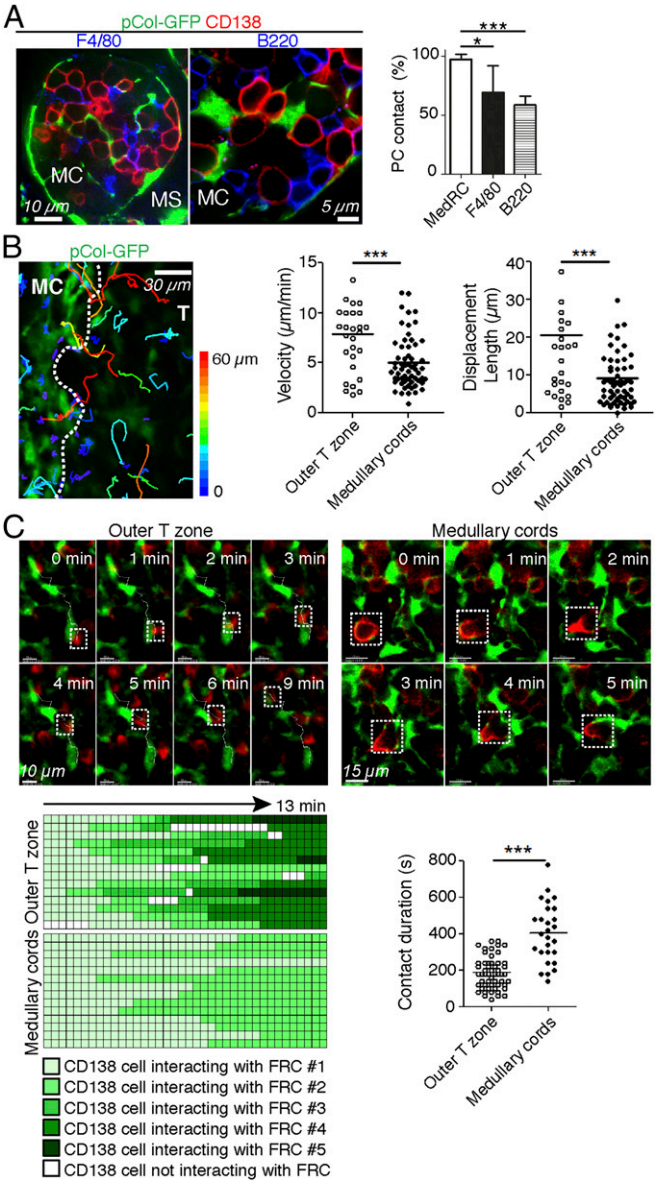

Fig. 4. Medullary FRCs are a major component of the plasma cell niche. (*A* and *B*) Immunofluorescence images of activated pLNs with MC areas being highlighted. (*A*) Confocal microscopy of activated pLNs (SRBC d7) from pCol-GFP mice stained with the antibodies indicated. (*Right*) Frequency of PCs in contact with F4/80$^+$ and B220$^+$ cells. Values are mean ± SD of three to five experiments in which conjugates were scored from six to nine LN slices. (*B* and *C*) Localization and migration of endogenous PBs/PCs in vibratome sections of viable activated pLNs from pCol-GFP mice. (*B*) Tracks of individual endogenous PBs/PCs in relation to GFP$^+$ FRCs. Tracks are color coded according to the extent of PB/PC displacement. Graphs at *Right* show velocities and displacement lengths of PBs/PCs. Values are from three experiments in which cells were monitored from three to five LN slices. See also Movie S3. (*C*) Motile behavior of PBs/PCs relative to GFP$^+$ FRCs. (*Top*) Snapshots are shown at various time intervals for the same zone and cells. The trajectory of PBs/PCs in the outer T zone was superimposed over fluorescence images. See also Movies S4 and S5. (*Bottom Left*) Graphic representation of interactions between PBs/PCs and GFP$^+$ FRCs. Each row corresponds to an individual PB/PC, and the periods of contact with FRCs are colored with different shades of green corresponding to different FRC partners and white corresponding to no FRC partner being visible. Graph at *Bottom Right* summarizes the average contact time of PBs/PCs with their FRC partners. *$P < 0.05$, ***$P < 0.001$.

cells within activated LNs, including MedRCs but not TRCs, suggesting that IL-6 directly or indirectly regulates the number of MC niches (*SI Appendix*, Fig. S6*B*). OVA-specific IgM and IgG levels in the serum were approximately twofold reduced in IL-6–deficient mice (*SI Appendix*, Fig. S6*C*). Strikingly, OVA-specific IgG produced in cultures from IL-6–deficient LNs were almost 10-fold reduced at both time points investigated and correlated well with the rare occurrence of IgG$^+$ PBs/PCs, while the local IgM response was hardly affected (Fig. 6 *A* and *B*). This striking scarcity of IgG$^+$ PCs raised the possibility that PCs in IL-6 KO mice have defects either in their migration or retention in MCs, where they complete their maturation into PCs or in their survival. In IL-6$^{-/-}$ mice, the localization and clustering of CD138$^+$ PCs next to MedRCs was unaltered (*SI Appendix*, Fig. S6*D*). Similarly, IL-6 neutralization had no effect on endogenous PC localization in MCs and no or minor effects on their velocity and spatial displacement (Fig. 6 *C* and *D* and Movie S7). Thus, IL-6 may primarily serve as a factor driving the development and/or survival of PBs/PCs, including possibly a role in isotype switching.

Medullary FRCs and Macrophages Promote PC Survival via IL-6 Production. Genetic tools to selectively manipulate MedRCs in vivo are currently lacking. Therefore, we turned to in vitro coculture assays to test whether MedRCs and innate immune cells are capable of regulating PB/PC homeostasis. While all purified PBs/PCs died when cultured alone for 3 d, 10–20% of PBs/PCs were rescued in presence of FRCs isolated from activated LNs to an extent similar to recombinant IL-6 (Fig. 7*A*). This PB/PC rescue involved very little PB proliferation in vitro (*SI Appendix*, Fig. S7*A*), indicating that this assay is mainly a readout for PC survival. PC numbers were preserved when PCs were separated from FRCs by a Transwell filter, or when PCs were cultured with FRC-conditioned medium, suggesting the survival factor is soluble rather than membrane bound (Fig. 7*A*). FRC-mediated PC survival was blocked almost entirely by IL-6 neutralizing antibodies but not by inhibitors of BAFF, APRIL, or CXCL12 (*SI Appendix*, Fig. S7*B*). However, a marked drop in *baff*, *april*, and *cxcl12* expression was noted in cultured FRCs, with minor effects for IL-6, which may be lost later on, as indicated by the low levels observed in the FRC line pLN2 (*SI Appendix*, Fig. S7*C*). Next, the various LN cell types were FACS sorted and tested in their capacity to mediate PC survival. MedRCs and macrophages were much more efficient in mediating PC survival compared with sorted TRCs and DCs, with no PC survival observed in LECs/BECs or T/B lymphocyte cocultures (Fig. 7*B*). PC survival by MedRCs, macrophages, or DCs was almost exclusively mediated by IL-6, as was their capacity to boost IgM and, more impressively, IgG production (Fig. 7 *C* and *D*). Combining the various cell types, each in suboptimal numbers, showed synergistic effects on PC survival and additive effects on IgG but not IgM secretion, with most of the effects mediated by IL-6 (Fig. 7*E* and *SI Appendix*, Fig. S7*D*). Interestingly, MedRCs seem to be more efficient in promoting IgM/G secretion by PCs than macrophages or DCs, also indicating that PC survival is not predictive of Ig secretion levels, which may depend on high IL-6 levels or additional factors. Collectively, these data demonstrate that MedRCs—together with myeloid cells—not only form physical niches for PCs, but also secrete factors capable of mediating PC survival and function.

Discussion

In the current study, we characterized a new fibroblast subset that we termed MedRCs, as it is present as reticular cell network throughout the medullary cords and is phenotypically and functionally distinct from TRCs and MRCs. MedRCs form niche-like structures in which PCs and innate immune cells reside. In addition, they are a rich source of various factors that can promote PB/PC migration, localization, survival, and function. We therefore propose that MedRCs are an important component of PC niches inside LNs and thereby positively regulate early humoral immunity.

The combination of two surface markers, MAdCAM and BP3, allowed us to distinguish murine MedRCs from TRCs and MRCs. This classification was largely confirmed by intracellular staining for CCL21 and CXCL13 proteins that were absent in

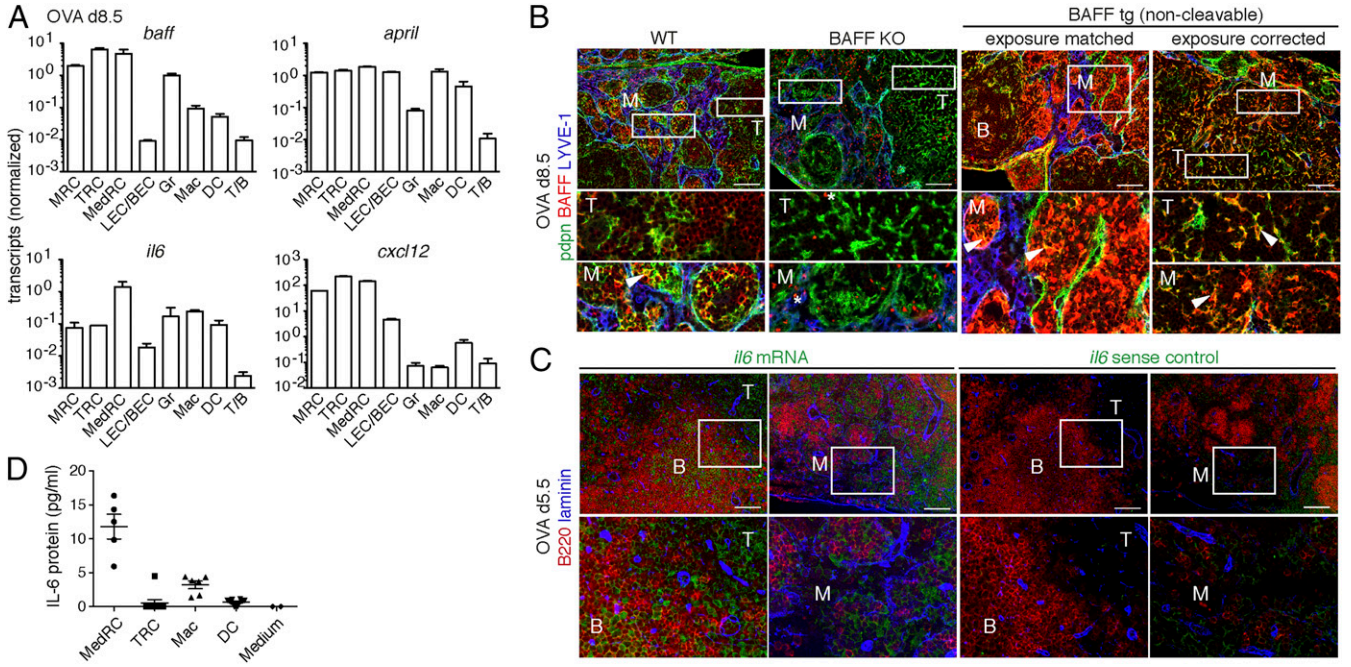

Fig. 5. Medullary FRCs express high levels of plasma cell survival factors. Mice were immunized with OVA/Mont and the expression of PC survival factors analyzed in draining pLNs. (*A*) The transcript levels of *baff*, *april*, *il6*, *and cxcl12* were assessed in cells sorted from fully digested pLNs as shown in Fig. 2*A* and *SI Appendix*, Fig. S5*A*. T/B lymphocytes were CD19$^+$ or TCRβ^+. (means ± SEM, naive $n = 2$, OVA $n = 4$). (*B*) Immunofluorescence staining of activated pLNs from WT, uncleavable BAFF transgenic, and BAFF KO mice for BAFF expression (red) on FRCs and LECs in medulla. Arrows point to BAFF$^+$ TRCs and MedRCs. Stars indicate staining artifacts due to high endogenous HRP in BAFF KO mice. $n = 3$. (*C*) ISH analysis of *il6* transcript or the sense control. The boxed areas are represented at higher magnification in the row below. (Scale bar, 100 μm.) $n = 3$. (*D*) ELISA for IL-6 protein levels in the supernatant of the indicated cell types sorted from d5 OVA/Mont-immunized pLNs and cultured for 18 h. Values were normalized for 10,000 cells. $n = 4$–9. Number of experiments: one (*A*), two (*D*), and two to four (*B* and *C*).

MedRCs, but allowed a further functional subdivision of TRCs and MRCs at the single cell level. Around 60% of TRCs express CCL21, consistent with previous observations (10, 20, 29, 30). TRCs also comprise around 15% CXCL13$^+$CCL21$^-$ cells, explaining the high level of *cxcl13* transcripts observed by us and others among pdpn$^+$ FRCs (20, 31), as well as *cxcl13* expression still found in follicles of FDC-depleted mice (32). Given the follicular localization of CXCL13 protein, these cells are likely to reside in the outer B cell follicle (21) and possibly coexpress BAFF (22), the Notch-ligand DL-4 (33), and enzymes generating the chemoattractant oxysterol (20). We propose to call them "B zone reticular cells" (BRCs) (*SI Appendix*, Fig. S7*E*). Our unbiased flow cytometric clustering analysis (TSNe) points to a total of at least seven phenotypically distinct fibroblast-like cell types inside LNs, not including the different CD35$^+$ FDC types and pdpn$^-$CD31$^-$ (double negative or DN) fibroblastic cells that were gated out from this analysis. Notably, these seven cell clusters appear to form a continuum that could reflect the zones as well as transitions between zones where specific processes, such as T–B collaboration or PB differentiation may occur (2, 34). A recent report based on single cell RNA sequencing of lymph node fibroblasts points to nine transcriptionally distinct populations, including the Inmt$^+$ stromal cells which most likely correspond to our MedRC subset (35). The exploration of these presumably different cell types or cell states, their relationship and regulation, as well as their respective function will be an important area for the future.

The MedRCs described here are numberwise a relatively large population within naive and activated LNs and have previously been considered together with their T zone counterparts. They include as a subset the recently described CD34$^+$ perivascular FRCs with precursor potential (30, 35). Importantly, MedRCs express little T and B zone chemokines, while producing CXCL12 at levels comparable to TRCs, consistent with high CXCL12-reporter expression in most LN FRCs (24). Given the prevalence of CXCL12 expression in sorted MedRCs compared with other MC cell types, along with the lacking expression in innate immune cells (8), we propose that MedRCs are the major local source of this chemokine along with blood vessels (24). MedRCs may therefore contribute to the medullary localization of CXCR4$^+$ cells which do not express much CCR7 and CXCR5, including PCs (2, 14), granulocytes, and macrophages, thereby generating the distinct cellular composition of MCs. CXCR4$^{-/-}$ PBs/PCs fail to localize appropriately within MCs (2), suggesting that cells excluded from T and B cell zones need CXCL12 cues to either migrate deeper into the MCs or to be retained in this region. Consistent with it, pertussis toxin treatment of mice reduced PC accumulation in MCs but most PB migration appeared to be nondirectional, similar to previous evidence (28). In vitro, PBs migrate toward CXCL12 gradients in a pertussis toxin-dependent manner (2, 14). Therefore, we propose that PBs which have reached the outer T zone are either attracted or retained by the CXCL12-expressing MedRCs. Additional factors, like accessible matrix fibers enriched within MCs (36), may also contribute to PBs/PCs adhesion and retention.

Fooksman et al. (28) have described the persistent linear tracks of PBs in the LN T zone followed by the slower and much more confined migration of PBs/PCs once they have reached MCs (37). We confirm these findings, and propose that the different migration strategy can be explained at least in part by PBs/PCs being physically guided initially by the TRC and later by the MedRC network, similar to the reported naive lymphocyte migration along TRCs and FDCs (17). The molecular basis for this PB crawling along the FRC networks remains to be defined, but may include ICAM-1 on FRCs (28). While the clearly decreased displacement of PCs relative to PBs is probably due to their terminal differentiation and therefore intrinsic changes, our results suggest that both the spatial organization and morphology of MedRCs may also contribute. The FRC network is denser in MCs than T zones. Relative to TRCs, MedRCs are less reticular and more stellate, presumably because they enwrap less the

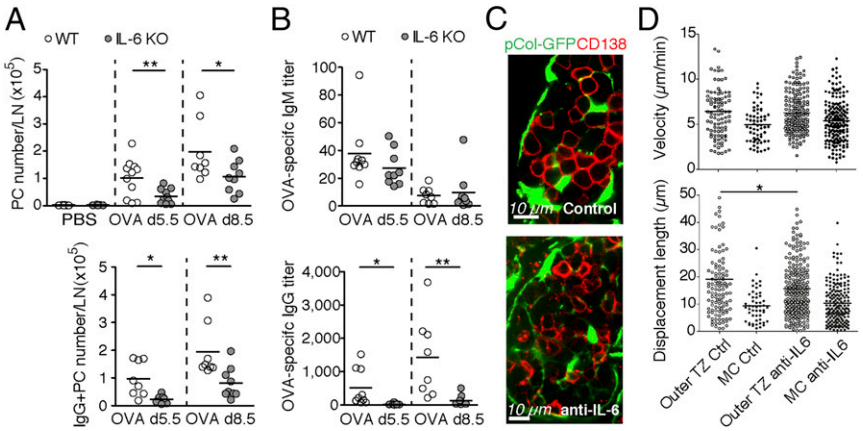

Fig. 6. IL-6 drives plasma cell differentiation or survival but not homing in activated lymph nodes. Cell suspensions of pLNs from WT or IL-6 KO mice (OVA/Mont d0, d5.5, or d8.5) were either analyzed ex vivo by FACS for the number of PCs and intracellular IgG$^+$ PCs per pLN (*A*) or for the titer of OVA-specific IgM/G measured in the supernatant of total pLN cells cultured for 3 d (*B*); n = 7–13. Localization (*C*) and motility (*D*) (velocity and displacement length) of endogenous PCs/PBs were monitored by time-lapse confocal microscopy in live vibratome slices from activated (SRBC d6) pLNs of pCol-GFP mice treated either with neutralizing antibodies to IL-6 (anti-IL-6) or control antibodies (Ctrl). TZ, T zone; $n = 6$ mice. Number of pooled experiments: six (*A* and *B*) and two (*C* and *D*). See also *SI Appendix*, Fig. S6 and Movie S7. *$P < 0.05$, **$P < 0.01$.

matrix fibers (36). This arrangement might impede fast and linear PC migration, with the more accessible matrix potentially allowing increased PC adhesion.

The slow PC motility within MCs goes along with the long contact duration and large contact zones with MedRCs. The cavities of the MedRC network appear tailor made in size for allowing residence and signal recognition by single PCs. Therefore, the term "survival niche" seems very appropriate. This niche also includes B220$^+$ B cells and myeloid cells, with the role of macrophages and dendritic cells being controversially discussed (4, 8, 10–12). We have observed synergistic effects on PC survival when combining MedRCs with myeloid cells. This is in contrast to macrophage depletion experiments showing an enhanced extrafollicular PC response (12). We have also performed preliminary experiments to deplete MedRCs in a CCL19Cre × ROSA-DTR cross (in collaboration with Lucas Onder and Burkhard Ludewig, Kantonsspital St. Gallen, St. Gallen, Switzerland). This approach that depleted 50–75% of MedRCs was associated with a 30–50% reduction in PCs, and a strong reduction in IgM and IgG secretion by LN-resident PCs. In addition, PCs accumulated within the outer T zone, suggesting MedRCs and/or TRCs are important for late B cell differentiation and/or PC survival. However, most LN cell types were affected by this depletion, including most TRCs and thereby presumably also lymphocyte differentiation processes within T zones. Therefore, in future, rather than using depletion systems, mouse models need to be developed to selectively ablate expression of PC guidance and survival factors in MedRCs versus TRCs. Despite the current lack of appropriate mouse models, the many lines of evidence presented here are all consistent with the notion that MedRCs contribute significantly to PC niches inside LNs, both structurally and functionally. We propose a model in which the PC niche is composed of motile hematopoietic cells but also of a static fibroblast network (*SI Appendix*, Fig. S7*F*), reminiscent of bone marrow niches for long-lived PCs (4, 5). This mixed composition may increase the robustness of the humoral response while allowing a more elaborate regulation. Whether fibroblasts also contribute to PC niches in other tissues, including spleen and intestinal lamina propria, remains an interesting open question.

IL-6, BAFF, APRIL, and CXCL12 can promote PC survival in vitro (3, 4), while less is known about their relative role and expression in vivo (24, 38). Analysis of various sorted innate cells has failed to identify the source of BAFF and CXCL12 (8) consistent with bone marrow chimera experiments pointing to nonhematopoietic cells as BAFF source (9). We now provide strong evidence for MedRCs being the elusive source of both BAFF and CXCL12 within MCs, with BAFF expression being highly MedRC restricted both at the mRNA and protein levels, consistent with a recent report (34). This BAFF source is distinct from the less prominent one in the T and B zones. BAFF expressed by MedRCs is very likely to be sensed by the neighboring PCs enhancing their survival, while TRC-derived BAFF could contribute to the earlier differentiation and survival of B cell blasts. These two roles for BAFF are different from the recently proposed one for BRC-derived BAFF in naive B cell survival and follicular homeostasis (22). Our attempts at neutralizing BAFF during an ongoing response led to only a weak reduction in PC survival, comparable to the one recently reported for early PC responses in mice deficient in hematopoietic April or IL-6 (38).

Myeloid cells were proposed to be a strong source for IL-6 (8) but surprisingly their depletion increased PC numbers (12). We found higher IL-6 expression in MedRCs than myeloid cells, both at the transcriptional and protein levels, similar to a recent report (34), with MedRCs being slightly more efficient in promoting IgM/G secretion by PCs, again in an IL-6–dependent manner. While lymphoid tissue fibroblasts were known as potent IL-6 sources that can mediate survival of PCs and hybridoma cells (7, 14, 15), the fibroblast subset colocalizing with PCs has to our knowledge not been sorted and tested ex vivo without passaging, as performed in this study. IL-6 is also known to regulate PC responses in vivo. However, previous publications have focused on late PC responses which most likely involve germinal center responses (6, 39, 40). Here we describe a 50% loss of the early extrafollicular PC generation in the absence of IL-6. Our reverse bone marrow chimera experiments using IL-6$^{-/-}$ and WT mice have failed to reveal any difference in the contribution of hematopoietic versus nonhematopoietic cells. These findings are consistent with our cocultures, where both MedRCs and myeloid cells promoted PC responses almost entirely via IL-6. While these findings establish that IL-6 produced by these cells can positively regulate PC survival and function, several signals were lost during culture, including BAFF and APRIL. It is also conceivable that the expression of negative regulators by myeloid cells was lost upon culture, which would explain the difference with some of the in vivo findings (12). Overall, our results are consistent with earlier proposals that in vivo PC survival may be controlled by a combination of factors, including IL-6, BAFF, and APRIL (3, 4). The precise roles of BAFF, APRIL, and IL-6 need to be further investigated in vivo using cell type-specific knockout mice, but the simultaneous presence of several B cell differentiation and PC survival factors as well as several niche cell types indicates a potential redundancy and robustness of the system (*SI Appendix*, Fig. S7*F*).

While most of our study focused on mouse tissues, we have provided here evidence for a similar fibroblast-based niche in MCs of human LNs. The markers described here and in a previous study (26) to distinguish human fibroblast subsets should be useful in future to sort and functionally define these cells, both in LNs and sites of chronic inflammation where PCs have been observed, like in rheumatoid arthritis joints or kidneys of lupus patients. Interestingly, in these settings fibroblast-like cells present within the lesions have been established as a major source of PC survival factors (41, 42), reminiscent of LN MedRCs and TRCs described in this study. In several B cell-mediated autoimmune diseases antibody-producing PCs are thought to reside in large numbers

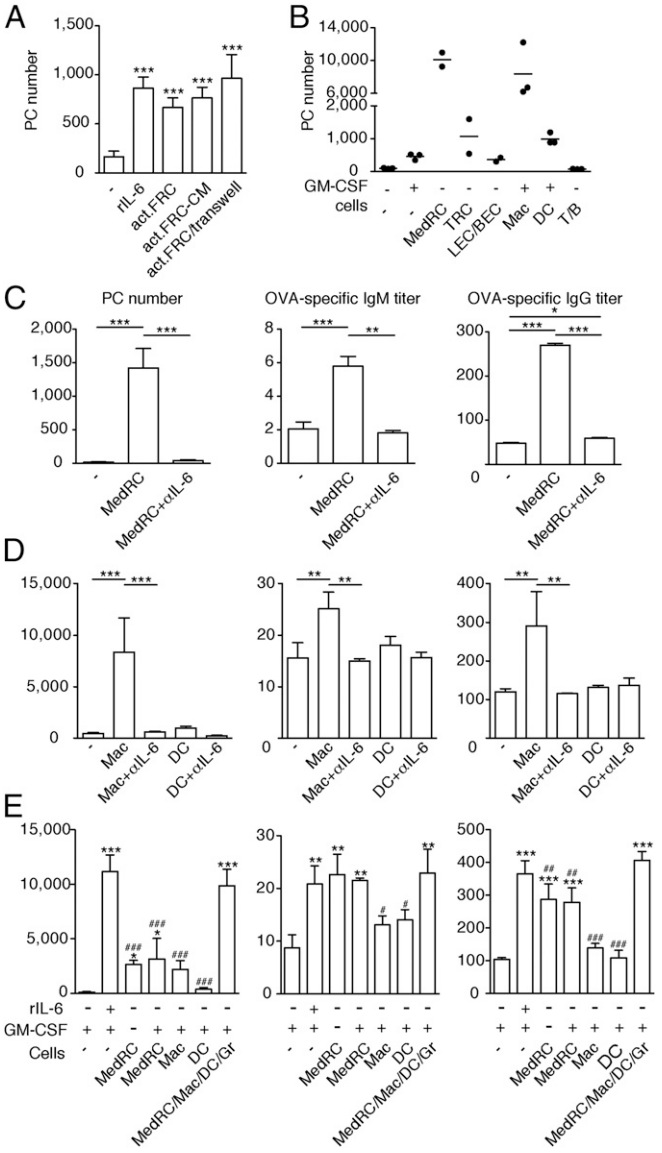

Fig. 7. Medullary FRCs, together with macrophages and dendritic cells, promote PC survival with a major role for IL-6. Activated pLNs (OVA/Mont d5-6) were used for MACS isolation of PBs/PCs and FACS sorting of potential support cells. PBs/PCs were cultured for 3 d in the indicated conditions followed by the analysis of surviving PCs by FACS ($B220^{low/-}CD138^{+}CD44^{+}IgM^{-}FSC^{hi}SSC^{hi}$) or of IgM/G antibody titers by ELISA. (*A*) Number of surviving PCs after culture in presence of rIL-6, a monolayer of total FRCs from d5.5 activated pLNs (act.FRC), conditioned medium (CM) from total act.FRC cultured for 3 d, or in presence of a Transwell separating act.FRCs from PCs. (*B*) Number of surviving PCs after culture in presence or absence of GM-CSF (to improve myeloid cell survival) or of a layer of the indicated cells. (*C–E*) PC numbers and IgM/G titers after cocultures in presence or absence of IL-6 neutralizing antibody or rIL-6; with or without MedRCs (*C*); macrophages (Mac), or DCs (*D*); in presence or not of GM-CSF along with the indicated cell type(s) (*E*). Gr, granulocytes. Error bars present SD ($n = 3–8$); $^{*/\#}P < 0.05$, $^{**/\#\#}P < 0.01$, $^{***/\#\#\#}P < 0.001$; in *F*, *, compared with PCs cultured with medium only (first column); #, compared with PCs cultured with MedRC/Mac/DC/Gr (last column). Shown results are representative of two (*A*, *C*, and *E*) or five (*B*) independent experiments.

inside the spleen and LNs, presumably in stable niches and contributing to pathogenesis. In such disease types, treatment with anti-CD20 antibodies (rituximab) often does not efficiently deplete PCs (43, 44). In contrast, therapies based on blocking BAFF/APRIL (Atacicept) or IL-6 have proven to be effective in reducing autoantibody levels and thereby autoimmune pathology (45, 46). These findings suggest that fibroblastic cells or their products are an interesting therapeutic target. Using this approach, pathological immune effector cells could be eliminated by destroying their survival niche. Conversely, boosting PC niches within LNs, spleen, or bone marrow may be a way of enhancing vaccine-induced humoral responses and memory.

Experimental Procedures

Mice and Immunization. C57BL/6 mice were from Harlan Olac and OT-I and OT-II mice from The Jackson Laboratory (bred to $CD45.1^{+}$ B6 mice). Other mice used were pCol-GFP transgenic (27), IL-6 knockout (39), BAFF knockout (47), noncleavable BAFF transgenic (48), and *plt/plt* (16). One million cells from LNs and spleen of OT-I and OT-II mice were injected i.v. into recipient mice which were immunized the following day s.c. with 50 μL OVA/Mont (1 mg/mL OVA; Sigma) containing 25% of Montanide ISA 25 (Seppic) above areas drained by inguinal, axillary, and brachial LNs (six injections per mouse) (25). Alternatively, mice were immunized the same way with 50 μL of sheep red blood cells (SRBCs) (Eurobio) leading to a comparable PC response. All mouse experiments were authorized by the Swiss Federal Veterinary Office (authorization no. 1612.2) and by the animal experimentation ethic committee of University Paris Descartes, Paris (CEEA34.ED.042.12).

FRC Isolation. Peripheral LNs (axillary, brachial, and inguinal) were dissected from killed mice, cut into small pieces, and digested for 30 min at 37 °C with gentle stirring in 1.5 mL DMEM (Gibco) containing collagenase IV (3 mg/mL), DNase I (40 μg/mL; Roche), $CaCl_2$ (3 mM) and 2% (vol/vol) FCS (16). Cells were then passed through a 40-μm strainer (Becton Dickinson), washed twice, and resuspended in DMEM/2% FCS.

Flow Cytometry and Cell Sorting. Cells were labeled as described previously (25) using Abs listed in *SI Appendix*, Table S1. Intracellular staining of chemokines was performed on surface-marked cells fixed with 2% PFA, then permeabilized and stained in 0.1% saponin in PBS. Rabbit anti-CCL21 and goat anti-CXCL13 were detected with Alexa 488- or 647-coupled secondary antibodies. Data were acquired on a LSRII (BD Biosystems) and analyzed with FlowJo (TreeStar). Cells were sorted with a FACSAria Ib, for RNA isolation directly into lysis buffer (RNeasy micro kit, Qiagen), or for cell culture into complete RPMI medium (Gibco).

MACS Purification and Survival Assays of Plasmablasts and Plasma Cells. pLNs of mice (OVA/Mont d6.5) passed through a 40-μm mesh were depleted of naive lymphocytes by panning (αB220, αTCRβ), then cell suspensions stained with anti-CD138 PE or biotin followed by anti-PE or streptavidin magnetic beads, respectively, and finally enriched by magnetic-activated cell sorting (MACS) (purity of 90–95%). Occasionally, they were labeled with 5 nM CSFE before the enrichment. Sorted stromal or hematopoietic cells were cultured overnight in 96-well plates followed by adding purified PCs at approximately a 5- to 10-fold higher number (1.2×10^4 or 6×10^4) and if indicated, inhibitors: αIL-6 (MP5-20F3, BioXcell), αAPRIL (Apry-1–1, Adipogen), αAPRIL and αBAFF (hTACI-Fc, Adipogen) or AMD3100 (inhibitor of CXCR4, Sigma). After 3 d, surviving PC numbers were determined by FACS.

ELISA Measurements of OVA-Specific IgM and IgG, and of IL-6 Protein Levels. Flat-bottom 96-well MaxiSorp plates (Nunc) were coated with 5 μg/mL OVA and blocked with 1% BSA in PBS. Serial dilutions of samples were added for 1 h and bound antibody was detected with biotinylated goat anti-mouse IgM or IgG (Invitrogen) followed by HRP-conjugated streptavidin (Jackson). Color development using 3,3′,5,5′-tetramethylbenzidine solution (Sigma) was measured at 450 nm with correction set at 550 nm. Relative antibody concentrations correspond to the dilution, giving an OD of 50%. IL-6 protein level was measured in the supernatant of cultured cells, according to the kit's instructions (eBioscience).

RNA Isolation and Quantitative Real-Time PCR. RNA was extracted using the RNeasy micro kit (Qiagen). First-strand cDNA synthesis, quantitative real-time PCR, primers, and normalization are as described previously (16) or shown in *SI Appendix*, Table S2.

Immunofluorescence Labeling of Tissue Sections. For murine tissue blocks, cryosections (8 μm) and labeling of naive or OVA/Mont-activated pLNs were as previously described (16). For details on antibodies, see *SI Appendix*, Table S1. Human pLNs were obtained from transplant patients after informed consent was obtained (ethics permit: CA/5192) and 5-μm cryostat sections were acetone fixed before staining. See *SI Appendix* for more details.

In Situ Hybridization. The *Ccl19*, *Ccl21*, *Cxcl13*, and *Cxcl12* "riboprobe" was cloned and used as described (16, 49). The nucleotides 35–767 of *Il6* (NM_031168.1) were used as a template for making a riboprobe. Cryosections of pLNs were treated as previously described (16). After in situ hybridization, tissue sections were stained with antibodies to B220 and laminin followed by fluorochrome-labeled secondary antibodies.

Microscopy and Image Analysis. Images were acquired either with an upright Zeiss Axioplan, a Zeiss SP5 confocal or a Leica DMI6000 spinning-disk confocal microscope. Images were treated using ImageJ (NIH), Adobe Photoshop, or Imaris (Bitplane). Certain images were stitched together manually using Photoshop software to cover the entire LN of interest with certain areas around it, lacking biological material, colored artificially in black. Imaging of fibrillar collagen within LNs of pCol-GFP mice was performed using SHG microscopy. To detect FRC-PC contacts, the colocalization tool in Imaris was used. Three-dimensional reconstruction of sequential *z* series was performed using the surface tool of Imaris. For additional information see *SI Appendix*.

Imaging of Plasma Cell Motility Within Live LN Slices. Live vibratome sections were stained for 15 min at 37 °C with APC-conjugated anti-CD138 (281.2) and washed thereafter. In some experiments, pCol-GFP mice were treated with either IL-6 neutralizing (MP5-20F3, 10 μg/mL) or control antibodies at days 2 and 5 after SRBC immunization. For details, see *SI Appendix*.

Statistical Analysis. Statistical analysis was determined with an unpaired two-tailed Student's *t* test or one-way ANOVA by Prism 5 (GraphPad). $*P < 0.05$, $**P < 0.01$, $***P < 0.001$.

Detailed experimental procedures can be found in *SI Appendix*.

Supplemental Information Appendix. Supplemental information includes additional experimental procedures, seven figures, seven movies, two additional tables, and references, and can be found as a pdf file with this article online.

ACKNOWLEDGMENTS. We thank Pierre Bourdoncle and Thomas Guilbert of the imaging facility of the Institut Cochin; Aubry Tardivel, Chen-Ying Yang, Gwilym Webb, as well as the histology, microscopy, and flow cytometry platforms in Lausanne, for advice and expert technical assistance; and Olivier Donzé (Adipogen) for the gift of BAFF/APRIL reagents. This study was supported by grants by the Swiss National Science Foundation (31003-146944/1 to S.A.L.), the Taiwan National Science Council (NSC 100-2917-I-564-005 to H.-Y.H.), the French Ligue Nationale Contre le Cancer (EL2014.LNCC/ED to E.D.), the Agence Nationale de la Recherche (CHEMIMMUN ANR-13-BSV3-0010 to A.R.-C.), and Cancer Research for Personalized Medicine (E.P.).

1. Mueller SN, Germain RN (2009) Stromal cell contributions to the homeostasis and functionality of the immune system. *Nat Rev Immunol* 9:618–629.
2. Cyster JG (2005) Chemokines, sphingosine-1-phosphate, and cell migration in secondary lymphoid organs. *Annu Rev Immunol* 23:127–159.
3. Oracki SA, Walker JA, Hibbs ML, Corcoran LM, Tarlinton DM (2010) Plasma cell development and survival. *Immunol Rev* 237:140–159.
4. Tangye SG (2011) Staying alive: Regulation of plasma cell survival. *Trends Immunol* 32:595–602.
5. Zehentmeier S, et al. (2014) Static and dynamic components synergize to form a stable survival niche for bone marrow plasma cells. *Eur J Immunol* 44:2306–2317.
6. Cassese G, et al. (2003) Plasma cell survival is mediated by synergistic effects of cytokines and adhesion-dependent signals. *J Immunol* 171:1684–1690.
7. Minges Wols HA, Underhill GH, Kansas GS, Witte PL (2002) The role of bone marrow-derived stromal cells in the maintenance of plasma cell longevity. *J Immunol* 169:4213–4221.
8. Mohr E, et al. (2009) Dendritic cells and monocyte/macrophages that create the IL-6/APRIL-rich lymph node microenvironments where plasmablasts mature. *J Immunol* 182:2113–2123.
9. Gorelik L, et al. (2003) Normal B cell homeostasis requires B cell activation factor production by radiation-resistant cells. *J Exp Med* 198:937–945.
10. Kumar V, et al. (2015) A dendritic-cell-stromal axis maintains immune responses in lymph nodes. *Immunity* 42:719–730.
11. Hebel K, et al. (2006) Plasma cell differentiation in T-independent type 2 immune responses is independent of CD11c(high) dendritic cells. *Eur J Immunol* 36:2912–2919.
12. Fooksman DR, Nussenzweig MC, Dustin ML (2014) Myeloid cells limit production of antibody-secreting cells after immunization in the lymph node. *J Immunol* 192:1004–1012.
13. Minges Wols HA, et al. (2007) The effects of microenvironment and internal programming on plasma cell survival. *Int Immunol* 19:837–846.
14. Ellyard JI, Avery DT, Mackay CR, Tangye SG (2005) Contribution of stromal cells to the migration, function and retention of plasma cells in human spleen: Potential roles of CXCL12, IL-6 and CD54. *Eur J Immunol* 35:699–708.
15. Jourdan M, et al. (2014) IL-6 supports the generation of human long-lived plasma cells in combination with either APRIL or stromal cell-soluble factors. *Leukemia* 28:1647–1656.
16. Link A, et al. (2007) Fibroblastic reticular cells in lymph nodes regulate the homeostasis of naive T cells. *Nat Immunol* 8:1255–1265.
17. Bajénoff M, et al. (2006) Stromal cell networks regulate lymphocyte entry, migration, and territoriality in lymph nodes. *Immunity* 25:989–1001.
18. Gretz JE, Anderson AO, Shaw S (1997) Cords, channels, corridors and conduits: Critical architectural elements facilitating cell interactions in the lymph node cortex. *Immunol Rev* 156:11–24.
19. Katakai T, et al. (2008) Organizer-like reticular stromal cell layer common to adult secondary lymphoid organs. *J Immunol* 181:6189–6200.
20. Yi T, et al. (2012) Oxysterol gradient generation by lymphoid stromal cells guides activated B cell movement during humoral responses. *Immunity* 37:535–548.
21. Mionnet C, et al. (2013) Identification of a new stromal cell type involved in the regulation of inflamed B cell follicles. *PLoS Biol* 11:e1001672.
22. Cremasco V, et al. (2014) B cell homeostasis and follicle confines are governed by fibroblastic reticular cells. *Nat Immunol* 15:973–981.
23. Abe J, et al. (2012) B cells regulate antibody responses through the medullary remodeling of inflamed lymph nodes. *Int Immunol* 24:17–27.
24. Bannard O, et al. (2013) Germinal center centroblasts transition to a centrocyte phenotype according to a timed program and depend on the dark zone for effective selection. *Immunity* 39:912–924.
25. Yang CY, et al. (2014) Trapping of naive lymphocytes triggers rapid growth and remodeling of the fibroblast network in reactive murine lymph nodes. *Proc Natl Acad Sci USA* 111:E109–E118.
26. Link A, et al. (2011) Association of T-zone reticular networks and conduits with ectopic lymphoid tissues in mice and humans. *Am J Pathol* 178:1662–1675.
27. Yata Y, et al. (2003) DNase I-hypersensitive sites enhance alpha1(I) collagen gene expression in hepatic stellate cells. *Hepatology* 37:267–276.
28. Fooksman DR, et al. (2010) Development and migration of plasma cells in the mouse lymph node. *Immunity* 33:118–127.
29. Luther SA, Tang HL, Hyman PL, Farr AG, Cyster JG (2000) Coexpression of the chemokines ELC and SLC by T zone stromal cells and deletion of the ELC gene in the plt/plt mouse. *Proc Natl Acad Sci USA* 97:12694–12699.
30. Sitnik KM, et al. (2016) Context-dependent development of lymphoid stroma from adult CD34(+) adventitial progenitors. *Cell Rep* 14:2375–2388.
31. Malhotra D, et al.; Immunological Genome Project Consortium (2012) Transcriptional profiling of stroma from inflamed and resting lymph nodes defines immunological hallmarks. *Nat Immunol* 13:499–510.
32. Wang X, et al. (2011) Follicular dendritic cells help establish follicle identity and promote B cell retention in germinal centers. *J Exp Med* 208:2497–2510.
33. Fasnacht N, et al. (2014) Specific fibroblastic niches in secondary lymphoid organs orchestrate distinct Notch-regulated immune responses. *J Exp Med* 211:2265–2279.
34. Zhang Y, et al. (2018) Plasma cell output from germinal centers is regulated by signals from Tfh and stromal cells. *J Exp Med* 215:1227–1243.
35. Rodda LBL, et al. (2018) Single-cell RNA sequencing of lymph node stromal cells reveals niche-associated heterogeneity. *Immunity* 48:1014–1028.e6.
36. Ushiki T, Ohtani O, Abe K (1995) Scanning electron microscopic studies of reticular framework in the rat mesenteric lymph node. *Anat Rec* 241:113–122.
37. Luther SA (2010) Plasma cell precursors: Long-distance travelers looking for a home. *Immunity* 33:9–11.
38. McCarron MJ, Park PW, Fooksman DR (2017) CD138 mediates selection of mature plasma cells by regulating their survival. *Blood* 129:2749–2759.
39. Kopf M, Herren S, Wiles MV, Pepys MB, Kosco-Vilbois MH (1998) Interleukin 6 influences germinal center development and antibody production via a contribution of C3 complement component. *J Exp Med* 188:1895–1906.
40. Wu Y, et al. (2009) IL-6 produced by immune complex-activated follicular dendritic cells promotes germinal center reactions, IgG responses and somatic hypermutation. *Int Immunol* 21:745–756.
41. Noss EH, Brenner MB (2008) The role and therapeutic implications of fibroblast-like synoviocytes in inflammation and cartilage erosion in rheumatoid arthritis. *Immunol Rev* 223:252–270.
42. Wang W, et al. (2014) Long-term B cell depletion in murine lupus eliminates autoantibody-secreting cells and is associated with alterations in the kidney plasma cell niche. *J Immunol* 192:3011–3020.
43. Shlomchik MJ (2008) Sites and stages of autoreactive B cell activation and regulation. *Immunity* 28:18–28.
44. Mahévas M, Michel M, Weill JC, Reynaud CA (2013) Long-lived plasma cells in autoimmunity: Lessons from B-cell depleting therapy. *Front Immunol* 4:494.
45. Mackay F, Schneider P (2009) Cracking the BAFF code. *Nat Rev Immunol* 9:491–502.
46. Kopf M, Bachmann MF, Marsland BJ (2010) Averting inflammation by targeting the cytokine environment. *Nat Rev Drug Discov* 9:703–718.
47. Schiemann B, et al. (2001) An essential role for BAFF in the normal development of B cells through a BCMA-independent pathway. *Science* 293:2111–2114.
48. Bossen C, et al. (2011) Mutation of the BAFF furin cleavage site impairs B-cell homeostasis and antibody responses. *Eur J Immunol* 41:787–797.
49. Hargreaves DC, et al. (2001) A coordinated change in chemokine responsiveness guides plasma cell movements. *J Exp Med* 194:45–56.